

## Hidden phases with neuromorphic responses and highly enhanced piezoelectricity in an antiferroelectric prototype

Sergey Prosandeev,<sup>1</sup> Sergei Prokhorenko,<sup>1</sup> Yousra Nahas,<sup>1</sup> Yali Yang,<sup>2</sup> Changsong Xu<sup>1</sup>,<sup>1</sup> Julie Grollier,<sup>3</sup> Diyar Talbayev<sup>1</sup>,<sup>4</sup> Brahim Dkhil,<sup>5</sup> and L. Bellaïche<sup>1</sup>

<sup>1</sup>*Physics Department and Institute for Nanoscience and Engineering, University of Arkansas, Fayetteville, Arkansas 72701, USA*

<sup>2</sup>*International Centre for Quantum and Molecular Structures, Physics Department, Shanghai University, Shanghai 200444, China*

<sup>3</sup>*Unité Mixte de Physique, Centre National de la Recherche Scientifique, Thales, Université Paris-Saclay, 91767 Palaiseau, France*

<sup>4</sup>*Department of Physics and Engineering Physics, Tulane University, 6400 Freret Street, New Orleans, Louisiana 70118, USA*

<sup>5</sup>*Laboratoire Structures, Propriétés et Modélisation des Solides, CentraleSupélec, Université Paris-Saclay,*

*Centre National de la Recherche Scientifique UMR8580, 91190 Gif-sur-Yvette, France*



(Received 29 March 2021; accepted 10 March 2022; published 28 March 2022)

An atomistic first-principles-based effective Hamiltonian is used to study the response of a prototype of antiferroelectric materials, namely, the perovskite sodium niobate system, to the application of terahertz electric pulses. So-called hidden phases are discovered due to such ultrafast field excitation. These phases are homogeneous in nature, and correspond to local minima of energy. In addition to improved piezoelectric responses, they also possess controllable magnitude of the electric polarization, leading to possible applications of antiferroelectrics for ultrafast neuromorphic computing.

DOI: [10.1103/PhysRevB.105.L100101](https://doi.org/10.1103/PhysRevB.105.L100101)

Antiferroelectrics are rich systems [1–6] that are attractive for energy storage (see, e.g., Refs. [7,8] and references therein) and for which the microscopic interactions responsible for their antipolar arrangement and properties have been intensively debated [3]. Among the antiferroelectric (AFE) compounds, sodium niobate  $\text{NaNbO}_3$  (NNO) has the most complex phase diagram since it has been reported to exhibit seven crystallographic phases when cooling it down [2,9]. Apart from the high-temperature cubic phase, all the other six thermodynamically stable states possess tiltings of oxygen octahedra. In particular, the one at room temperature is additionally antiferroelectric and has been assigned the  $Pbcm$  symmetry while the ground state further adopts a spontaneous electric polarization within a  $R3c$  symmetry. Note that other experimental data and simulations measured and predicted the existence of other stable phases in NNO [10–13]. Due to this unusual variety of known phases, it may seem provocative to wonder if other phases still await to be discovered in NNO. In fact, recent remarkable works have revealed, in various materials, the existence of novel states: the so-called hidden states, that are phases being usually *not* thermodynamically accessible (i.e., they are not reachable by bias field or temperature change) but rather being activated via out-of-equilibrium processes. For instance, such hidden states have been optically induced in superconductors [14], colossal magnetoresistive manganites [15], charge-density-wave materials [16], and incipient ferroelectrics (FEs) [17,18]. The range of the excitations of such states is in the visible [16], midinfrared [14,15], and also terahertz intervals [17,19]. In particular, ferroelectricity was induced in a quantum-paraelectric  $\text{SrTiO}_3$  by a terahertz optical pulse [17], while ferroelectricity is not accessible in this material under cooling without the field.

One may thus legitimately ask if the hidden phases can be created in NNO too, by, e.g., applying terahertz electric-field pulses. Such possibility is also exciting for the three following reasons. First of all, and as demonstrated in a very recent work on the  $\text{Pb}(\text{Mg}, \text{Nb})\text{O}_3$  (PMN) relaxor system [20], the hidden phases can be put in use to design neuromorphic computing [21]. This is because they enable one to go continuously from an initial to the final state via the hidden phases, giving rise to features needed for neuromorphic computing (such as the existence of the nonvolatile multiple states and nonvolatile control). If the hidden phases will be found in NNO, the antiferroelectrics will have to be considered as integral members of the neuromorphic materials (we are not aware of any previous work demonstrating that antiferroelectrics can emulate the features of neuromorphic computing). Second, one may also wonder if these hypothetical hidden phases in NNO have the same nature as those in PMN. Namely, what are the hidden states bridging the antiferroelectric and ferroelectric phases in NNO? Note that, in the experimentally measured thermodynamically stable electric field temperature phase diagram of NNO [22] and in our calculations (to be shown elsewhere), there are no hidden states at equilibrium and only sharp transitions between the AFE and FE phases have been observed. Third, are these hidden states having local minima in this structural path, and do these states show enhanced physical properties [23]?

The aim of this Letter is to employ an atomistic approach, combined with the development of an algorithm to extract the structural path having the minimal elastic energy, to reveal that (1) the hidden states in the antiferroelectric NNO have the local and stable energy minima and possess large piezoelectric coefficients (these states indeed show up in NNO under

terahertz electric pulses) and (2) NNO has all ingredients of the neuromorphic architecture. The present Letter thus establishes our computational framework as an important tool to discover novel neuromorphic materials and predicts their emergence and features under a terahertz train of the electric pulses.

In the present Letter, we employ the effective Hamiltonian developed and detailed for NNO in Ref. [13]. In addition to the inhomogeneous and homogeneous strains, this Hamiltonian has two other degrees of freedom in each five-atom unit cell  $i$ : (i) the local mode  $\mathbf{u}_i$ , which is directly proportional to the local electric dipole moment centered on the Na ion in the primitive unit cell  $i$  [24,25], and (ii) a Nb-centered pseudovector  $\boldsymbol{\omega}_i$ , for which the direction is the axis about which the oxygen octahedron of cell  $i$  rotates while the magnitude is the angle of such rotation [26] (these tiltings of the oxygen octahedra are often called antiferrodistortive motions). This effective Hamiltonian provides several phases in NNO, consistent with the measurements [27–31]. The  $R3c$  rhombohedral ferroelectric phase is found to be the ground state of this Hamiltonian, as also in agreement with observations [32,33]. A complex AFE orthorhombic state is also predicted to be of slightly higher energy than  $R3c$ , which is in line with the experimental report [9] of a  $Pbcm$  phase between 693 and 173 K on cooling, before NNO acquires the  $R3c$  shape. To characterize such an AFE  $Pbcm$  state (but also other states later on), let us define the following quantities in the reciprocal space:

$$u_{\mathbf{k},\alpha} = \frac{1}{N} \left| \sum_i u_{i,\alpha} \exp(i\mathbf{k} \cdot \mathbf{R}_i) \right|, \quad (1)$$

$$\omega_{\mathbf{k},\alpha} = \frac{1}{N} \left| \sum_i \omega_{i,\alpha} \exp(i\mathbf{k} \cdot \mathbf{R}_i) \right|, \quad (2)$$

where  $\mathbf{k}$  is a wave vector belonging to the cubic first Brillouin zone,  $\alpha$  denotes the Cartesian components, and the sums run over all  $N$  five-atom sites in the supercell. Note that  $x$ ,  $y$ , and  $z$  axes are chosen along the pseudocubic [100], [010], and [001] directions, respectively. The  $Pbcm$  phase is characterized by several  $\mathbf{k}$  points for which these Fourier transforms have significant weights. Two of them are associated with modes possessing oxygen octahedral tiltings [34]: in  $2\pi/a$  units, they are  $R = (\frac{1}{2}, \frac{1}{2}, \frac{1}{2})$  for the  $x$  and  $y$  components of  $\boldsymbol{\omega}_{\mathbf{k},\alpha}$  and  $T = (\frac{1}{2}, \frac{1}{2}, \frac{1}{4})$  for the  $z$  component of  $\boldsymbol{\omega}_{\mathbf{k},\alpha}$ . The corresponding  $\omega_{\mathbf{k},\alpha}$  will thus be denoted as  $\omega_{R,x} = \omega_{R,y}$  and  $\omega_{T,x}$  in the following for the  $Pbcm$  phase.  $\omega_{R,x}$  (respectively,  $\omega_{R,y}$ ) characterizes the antiphase tilting about the  $x$  axis (respectively,  $y$  axis), while  $\omega_{T,z}$  quantifies the “++−−” periodic arrangement of the tilting pattern along the  $z$  axis. Besides tilting, the  $Pbcm$  distortion has  $\Delta_5$  antiferroelectric-type displacements with a  $\mathbf{k}$  vector located at the  $(0, 0, \frac{1}{4})$  point called  $\Delta$ . The resulting  $u_{\mathbf{k},\alpha}$ ’s are denoted as  $u_{\Delta,x} = u_{\Delta,y}$  and correspond, in our effective Hamiltonian scheme, to the “+0-0” periodic pattern [34] of the  $x$  and  $y$  components of the Na-centered local modes, when moving along the  $z$  axis. Note that the combined existence of such antiferrodistortive and antipolar modes results from a trilinear coupling between these two types of motion [35] and makes  $Pbcm$  an example of a so-called nanotwin phase [36] with a periodicity of a four-lattice constant along the  $z$  axis.

Interestingly, the aforementioned effective Hamiltonian [13] predicted that the reported AFE and antiferrodistortive  $Pbcm$  state of NNO may in fact be of  $Pca2_1$  symmetry, that is, a phase that emerges from  $Pbcm$  by adding a polarization along the  $z$  axis and a weak antipolar displacement  $u_{X,z}$  along the same axis and associated with the  $X$  point  $(0, 0, \frac{1}{2})$ . Note that this polarization is found in the simulations of Ref. [13] rather small around room temperature, namely, of  $0.02 \text{ C/m}^2$ , that may explain why measurements reported a  $Pbcm$  symmetry rather than  $Pca2_1$  around 300 K. Note that some phases possessing a polarization in NNO at room temperature have been reported in Refs. [10–12].

Here, we employ this effective Hamiltonian [13] with molecular dynamics on  $12 \times 12 \times 12$  supercells, in order to explore the response of the  $Pca2_1$  phase to terahertz electric pulses at 100 K. This latter computational temperature should, in fact, be considered to rather be about 245 K since the effective Hamiltonian of Ref. [13] predicts that, upon heating, the cubic  $Pm\bar{3}m$  phase appears at 373 K to be compared with the measured value of 914 K (see Ref. [9]). As such, our chosen simulated temperature should correspond to a temperature regime for which the related  $Pbcm$  state has been experimentally reported. Note that some numerical parameters (namely, soft mode mass and moment of inertia) were obtained from density functional theory, as detailed in the Supplemental Material [37].

Moreover we apply, in the present molecular dynamics simulations, electric pulses along the [111] direction and of the form

$$\mathbf{E}_p(t) = E_0 \exp\left[-\frac{(t-t_0)^2}{\delta^2}\right] \cos[\omega(t-t_0)], \quad (3)$$

where  $E_0$  is the magnitude of the pulse,  $t$  is the time variable,  $t_0$  is the temporal position of the main maximum,  $\omega$  is the angular frequency, and  $\delta$  is the width of the Gaussian. This simple form of terahertz pulse is convenient to use in the simulations and rather close to those that are experimentally feasible [38].

Let us now choose a set of specific parameters representative of a terahertz pulse, namely,  $E_0 = 2.2\sqrt{3} \times 10^8 \text{ V/m}$ ,  $\delta = 0.4 \text{ ps}$ , and  $\nu = \omega/2\pi = 6 \text{ THz}$  in Eq. (3). Note that, due to Landauer’s paradox [39], the electric field in our simulations is usually larger as compared to experiments. For instance, a factor of 25 has been found for the  $R3c$  phase of  $\text{BiFeO}_3$  (see Ref. [40]). Note also that we repeat here such pulse every 8 ps, with the first pulse occurring at 5 ps, until the end of the simulations happening at 150 ps. We thus send a *train of pulses*. In Fig. 1, we present the result of our calculations for different physical quantities. More precisely, Fig. 1(a) displays the projection of the supercell average of the local modes along [111], that is,  $\langle u \rangle = \frac{1}{\sqrt{3}} (u_{\mathbf{k},x} + u_{\mathbf{k},y} + u_{\mathbf{k},z})$  with  $\mathbf{k}$  in Eq. (1) being the zone-center  $\Gamma$  point, as a function of time. Such quantity is thus directly proportional to the component of the polarization along the pseudocubic [111] direction. Furthermore, Fig. 1(b) shows Cartesian components of quantities related to oxygen octahedral tilting, that are the antiphase  $\omega_{R,x}$ ,  $\omega_{R,y}$ , and  $\omega_{R,z}$  but also the longer-period pattern along the  $z$  axis, as represented by  $\omega_{T,z}$ . Figures 1(c) and 1(d) display quantities related to antipolar displacements, namely,  $u_{X,z}$  at the  $X$  point, as well as  $u_{\Delta,x}$  and  $u_{\Delta,y}$  at the  $\Delta$  **k**

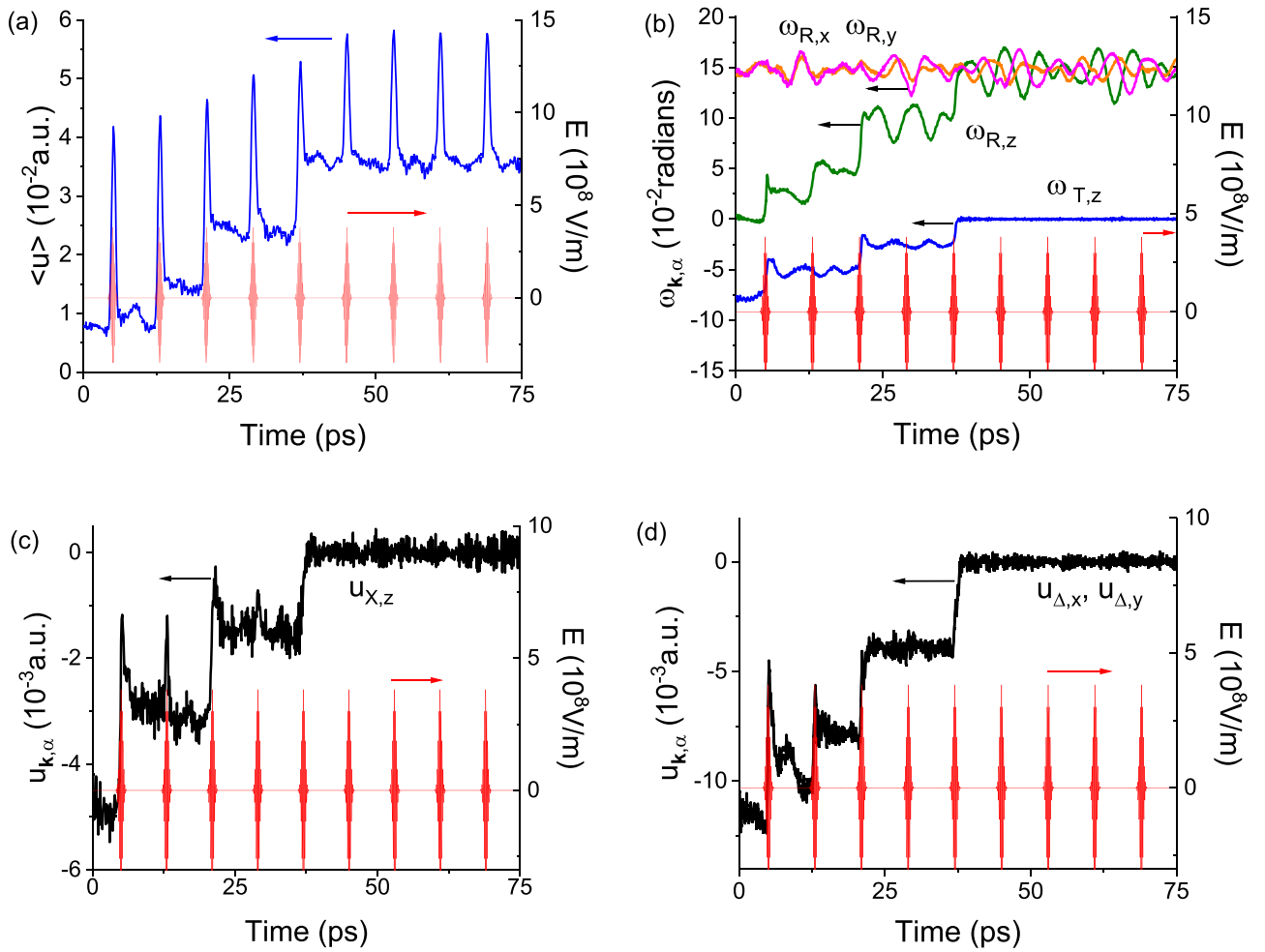


FIG. 1. Temporal evolution of (a)  $\langle u \rangle$ ; (b)  $\omega_{R,x}$ ,  $\omega_{R,y}$ ,  $\omega_{R,z}$ , and  $\omega_{T,z}$ ; (c)  $u_{X,z}$ ; and (d)  $u_{\Delta,x} = u_{\Delta,y}$  (see text for definition) of NNO subject to the train of electric pulses indicated via red lines.

point, respectively. Note that the patterns corresponding to all these quantities, allowing us to identify the space group of the corresponding phases, are schematized in the Supplemental Material (see Ref. [37] and Refs. [41–46] therein).

At  $t = 0$  s, the finite values of  $\langle u \rangle$ ;  $\omega_{R,x} = \omega_{R,y}$ ,  $\omega_{T,z}$ ,  $u_{X,z}$ ; and  $u_{\Delta,x} = u_{\Delta,y}$  are representative of our initial  $Pca2_1$  state. Strikingly, the first five pulses (at 5, 13, 21, 29, and 37 ps) result in several features: (i) an overall increasing polarization after each electric-field spike; (ii) the activation of  $\omega_{R,z}$  that is also strengthened after each of these pulses while  $\omega_{T,z}$  progressively decreases in magnitude; and (iii)  $u_{X,z}$  and  $u_{\Delta,x} = u_{\Delta,y}$ , that all experience their magnitude being reduced with respect to their initial value. These behaviors are associated with new hidden states of monoclinic  $Pc$  symmetry that we will detail below. Interestingly, a few picoseconds after the fifth pulse occurring at 37 ps, only the following several quantities are finite and slightly fluctuate in value in reaction to the subsequent applied pulses: (1)  $\langle u \rangle$  reaches a significant value larger than 0.035 in arbitrary units, corresponding to an electrical polarization of 0.32 C/m<sup>2</sup>; and (2)  $\omega_{R,x} = \omega_{R,y} = \omega_{R,z}$ , all adopting values about 0.15 rad, which thus indicates an antiphase tilting of  $\simeq 7.4$  deg about the [111] direction. In other words, after 37 ps, NNO now adopts a  $R3c$  state on average. Note that the effects of the parameters

defining the train of pulses on the results of Fig. 1 are reported in the Supplemental Material [37].

Let us now come back to the aforementioned different intermediate states of  $Pc$  symmetry, and check if they can also be stabilized once the electric field is withdrawn. For that, we repeat the calculations indicated in Fig. 1, but stop the train of electric pulses at a selected time and then pursue the molecular dynamics simulations until 150 ps under no more applied electric fields. The selected time was chosen to be 11, 17, and 35 ps and the result of these three different simulations (one for each selected time) is reported in Fig. 2—with the portion until 75 ps being shown, as similar to Fig. 1. Strikingly, Fig. 2 demonstrates that states of  $Pc$  symmetry continue to occur, and are stabilized, even when the pulses are turned off in these three different cases (Fig. 2 also shows results when the train of pulses is stopped at 42 ps, in which case the ferroelectric  $R3c$  state that had just been formed continues to happen even for times larger than 42 ps). This is remarkable when realizing that no such monoclinic  $Pc$  state has ever been previously reported in NNO, to the best of our knowledge. In fact, these presently discovered  $Pc$  states are examples of so-called hidden states. We also further found that our  $Pc$  states are homogeneous in nature, in the sense that they do not consist of a mixture of  $R3c$  clusters in one part of the system

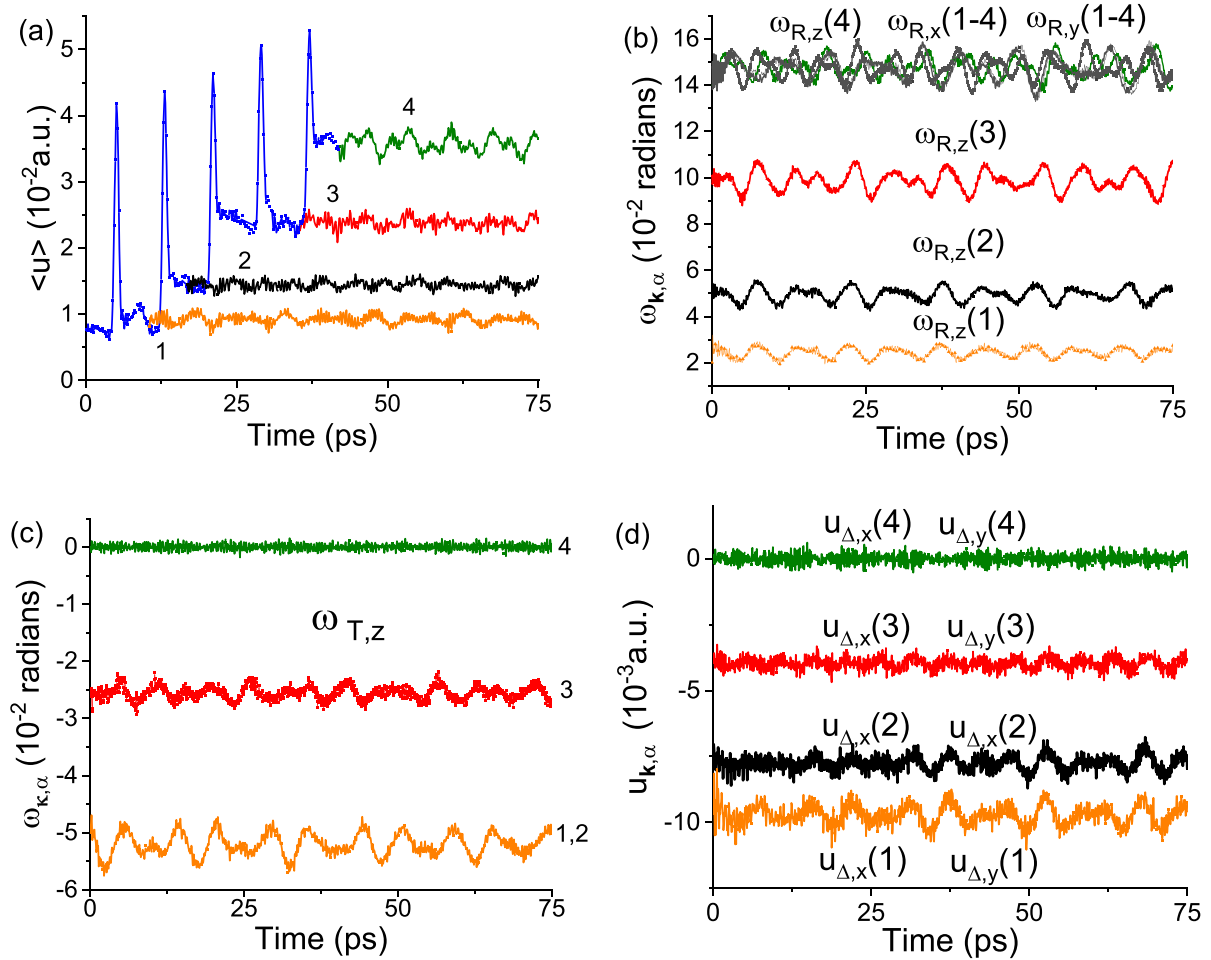


FIG. 2. Same as Fig. 1 but when the train of pulses is switched off at 11 ps (states 1), 17 ps (states 2), 35 ps (states 3), and 42 ps (states 4). Note that the zero of the time scale in panels (b)–(d) corresponds to the time at which the train of pulses has been switched off for these four different states. Panel (a) combines the plots of  $\langle u \rangle$  during the pulses (blue line) and the plots of  $\langle u \rangle$  after switching these pulses (one by one) off (orange, black, red, and olive lines). Panels (b)–(d) show the other modes only after switching the pulses off.

and of  $Pca2_1$  clusters in another part of the sample. In order to have a further insight into these  $Pc$  states, we developed an algorithm allowing us to perform climbing-image nudged elastic band (CNEB) calculations [47,48] within our effective Hamiltonian scheme [49,50], as detailed in the Supplemental Material [37]. Such calculations reveal that  $Pc$  states are intermediate states happening along the path with minimal energy bridging the  $Pca2_1$  and  $R3c$  states, with some of them being local energy minima. A similar conclusion is reached when conducting CNEB calculations but within the VASP [51–53] and USPEX [54–56] packages.

It is also important to realize that Fig. 2(a) further tells us that the magnitude of the electrical polarization can be controlled in these  $Pc$  states by stopping the train of pulses at different times. Practically, this polarization oscillates around values equal to 0.07, 0.14, 0.22, and 0.32 C/m<sup>2</sup> after turning off the electric field at 11, 17, 35, and 42 ps, respectively. Such different magnitudes also result in a tuning of physical properties, which is in line with the fact that hidden states can possess features leading to interesting applications [23]. For instance, when choosing indices 1 and 3 to correspond to the [100] and [001] pseudocubic direction, respectively, the  $d_{33}$

(respectively,  $d_{13}$ ) piezoelectric coefficient at 100 K increases with the increase of the local mode and adopts values of 247, 392, 406, and 412 (respectively,  $-22$ ,  $-37$ ,  $-84$ , and  $-209$ ) pC/N for the states for which the train of pulses has been switched off at 11, 17, 35, and 42 ps, respectively. These values are much larger in magnitude than those of 17 and 28 (respectively, 0.8 and  $-8$ ) pC/N for the  $d_{33}$  (respectively,  $d_{13}$ ) coefficient of the initial  $Pca2_1$  and final  $R3c$  states of Fig. 1, respectively. They are, in fact, of the same order of magnitude as those measured in the best lead-free piezoelectric compounds. Note that the Supplemental Material [37] also reveals how the strain is affected by the application of the train of pulses. Note also that, since we have used a Nosier-Hoover thermostat, effects, such as temperature change, were not taken into account here.

Let us now check if applying terahertz electric pulses in  $NaNbO_3$  can be of benefit for neuromorphic computing. For that, three key functions are needed.

(1) One is the capacity of the neuromorphic material to integrate input spikes. Interestingly, the gradual increase of polarization shown in Fig. 1(a) from the initial  $Pca2_1$  state to the final  $R3c$  state, via the intermediate  $Pc$  states, is a

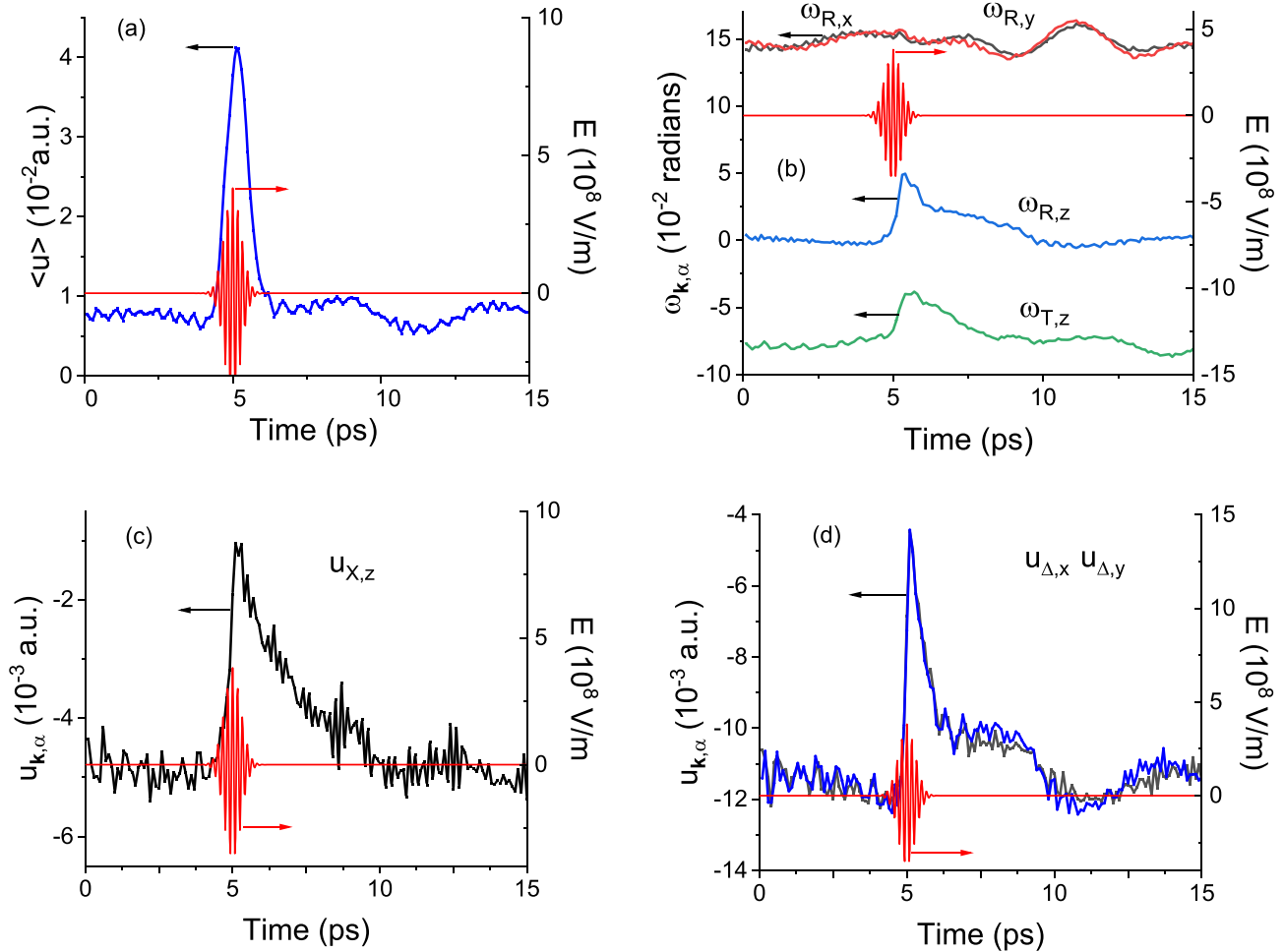


FIG. 3. Same as Fig. 1 but for a single pulse.

demonstration of such integration property of NNO. Note that the integration part is the most complicated one in complementary metal-oxide semiconductor and this is what we indeed demonstrated and explained in detail here.

(2) A second needed feature is the system possessing multiple nonvolatile states. The existence of such multiple states is evidenced in Figs. 1 and 2, thanks to the hidden phases of *Pc* symmetry.

(3) A third requirement is the ability of the compound to emit action potential. To check this possibility, we decided to apply to the *Pca2*<sub>1</sub> phase of NNO bulk a *single* terahertz pulse with the same parameters of Eq. (3) as in Fig. 1(a) and at the same temperature of 100 K.

The results are shown in Fig. 3. They reveal that NNO first responds to such single pulse by adopting an intermediate hidden phase of *Pc* symmetry before returning, after some time, to a state having the same symmetry as the initial one, that is, *Pca2*<sub>1</sub>. Such evolution is precisely the characteristics of an action potential [57]. In other words, NNO under terahertz electric pulses appears to have characteristics needed to serve as a basic element for a new neuromorphic architecture. Note also that two other requirements are typically needed for such latter architecture, namely, the reset and the firing/spiking. Regarding the reset, going back from the final *R3c* state of Figs. 1 and 2 to the initial *Pca2*<sub>1</sub> state is experimentally

possible by heating NNO to induce the transformation to *Pca2*<sub>1</sub> or other equilibrium states known in NaNbO3 and then cool down the system to reach back again the initial equilibrium *Pca2*<sub>1</sub> phase at our 100-K chosen temperature. Regarding the firing/spiking, it is important to realize that different neuromorphic models, such as spiking neural networks [58] or the leaked integration fire model [59], require the system to “fire” when a specific physical quantity is above a certain threshold. One striking feature of our results is that the hidden phases we presently discovered have different magnitude for their polarization [see Fig. 1(a)]. Hence, one can indeed set the system to fire when the polarization of these hidden states exceeds a certain value (note also that the polarization of these hidden states should not be perturbed by the readout since the voltage needed for such readout is typically small, and these hidden states correspond to given local minima in energy with specific values of polarization according to the Supplemental Material [37]).

It is also striking to realize that the typical frequencies of known memristive materials, e.g., in resistive switching, phase change, spintronics, and ferroelectric technologies, are below the gigahertz range [60–63], and having terahertz as characteristic frequencies for neuromorphic computing will result in ultrafast processing of data and lower energy consumption [64–69], which is of the utmost importance. It is also

interesting to recall that another terahertz neuromorphic material was recently proposed [20], namely, the relaxor  $\text{Pb}(\text{Mg}, \text{Nb})\text{O}_3$ , but the neuromorphic process was relying on another mechanism: the gradual evolution, increase, and then percolation of the local polar nanoregions that led to the occurrence of intermediate, *inhomogeneous* states while, in NNO, the nonvolatile multiple states are made of *homogeneous Pc* states being local energy minima. Such difference emphasizes the diversity that neuromorphic materials can adopt and extends their family members. We thus hope that the present Letter revealing the possibility of inducing hidden phases (having larger responses than the thermodynamically stable states) in the complex and antiferroelectric NNO system will be confirmed and broadens the fascinating fields of out-of-equilibrium physics and (ultrafast) neuromorphic architecture.

Sergey Prosandeev and L.B. acknowledge an Impact grant from the Arkansas Research Alliance, and ONR Grant No. N00014-21-1-2086. Sergei Prokhorenko and L.B. acknowledge the Vannevar Bush Faculty Fellowship from the U.S. Department of Defense. Y.N. and L.B. acknowledge DARPA Grant No. HR0011727183-D18AP00010 (TEE Program). D.T. acknowledges support from NSF for work on terahertz-driven ferroelectric dynamics under Grant No. DMR-1554866. B.D. would like to thank the French ANR through EXPAND Project No. ANR-17-CE24-0032. J.G. acknowledges support from Q-MEEN-C, an Energy Frontier Research Center funded by the U.S. Department of Energy, Office of Science, Basic Energy Sciences, under Grant No. DE-SC0019273, for work on neuromorphic computing with NNO.

- 
- [1] C. Kittel, *Phys. Rev.* **82**, 729 (1951).
- [2] F. Jona and G. Shirane, *Ferroelectric Crystals* (Pergamon Press, New York, 1962).
- [3] K. M. Rabe, in *Functional Metal Oxides: New Science and Applications*, edited by S. Ogale and V. Venkateshan (Wiley, New York, 2013).
- [4] A. K. Tagantsev, K. Vaideeswaran, S. B. Vakhrushev, A. V. Filimonov, R. G. Burkovsky, A. Shaganov, D. Andronikova, A. I. Rudskoy, A. Q. R. Baron, H. Uchiyama, D. Chernyshov, A. Bosak, Z. Ujma, K. Roleder, A. Majchrowski, J.-H. Ko, and N. Setter, *Nat. Commun.* **4**, 2229 (2013).
- [5] K. Patel, S. Prosandeev, and L. Bellaiche, *npj Comput. Mater.* **3**, 34 (2017).
- [6] K. Patel, S. Prosandeev, Y. Yang, B. Xu, J. Íñiguez, and L. Bellaiche, *Phys. Rev. B* **94**, 054107 (2016).
- [7] Z. Liu, T. Lu, J. Ye, G. Wang, X. Dong, R. Withers, and Y. Liu, *Adv. Mater. Technol.* **3**, 1800111 (2018).
- [8] B. Xu, J. Íñiguez, and L. Bellaiche, *Nat. Commun.* **8**, 15682 (2017).
- [9] I. Lefkowitz, K. Lukaszewicz, and H. D. Megaw, *Acta Cryst.* **20**, 670 (1966).
- [10] K. E. Johnston, C. C. Tang, J. E. Parker, K. S. Knight, P. Lightfoot, and S. E. Ashbrook, *J. Am. Chem. Soc.* **132**, 8732 (2010).
- [11] A. C. Sakowski-Cowley, K. Lukaszewicz, and H. D. Megaw, *Acta Cryst. B* **25**, 851 (1969).
- [12] S. I. Raevskaya, M. A. Malitskaya, C.-C. Chou, A. G. Lutokhin, I. P. Raevski, and V. V. Titov, *Phys. Status Solidi A* **216**, 1800972 (2019).
- [13] Y. Yang, B. Xu, C. Xu, W. Ren, and L. Bellaiche, *Phys. Rev. B* **97**, 174106 (2018).
- [14] D. Fausti, R. I. Tobey, N. Dean, S. Kaiser, A. Dienst, M. C. Hoffmann, S. Pyon, T. Takayama, H. Takagi, and A. Cavalleri, *Science* **331**, 189 (2011).
- [15] M. Rini, R. Tobey, N. Dean, J. Itatani, Y. Tomioka, Y. Tokura, R. W. Schoenlein, and A. Cavalleri, *Nature (London)* **449**, 72 (2007).
- [16] L. Stojchevska, I. Vaskivskiy, T. Mertelj, P. Kusar, D. Svetin, S. Brazovskii, and D. Mihailovic, *Science* **344**, 177 (2014).
- [17] X. Li, T. Qiu, J. Zhang, E. Baldini, J. Lu, A. M. Rappe, and K. A. Nelson, *Science* **364**, 1079 (2019).
- [18] T. F. Nova, A. S. Disa, M. Fechner, and A. Cavalleri, *Science* **364**, 1075 (2019).
- [19] M. Liu, H. W. Hwang, H. Tao, A. C. Strikwerda, K. Fan, G. R. Keiser, A. J. Sternbach, K. G. West, S. Kittiwatanakul, J. Lu, S. A. Wolf, F. G. Omenetto, X. Zhang, K. A. Nelson, and R. D. Averitt, *Nature (London)* **487**, 345 (2012).
- [20] S. Prosandeev, J. Grollier, D. Talbayev, B. Dkhil, and L. Bellaiche, *Phys. Rev. Lett.* **126**, 027602 (2021).
- [21] V. K. Sangwan and M. C. Hersam, *Nat. Nanotechnol.* **15**, 517 (2020).
- [22] L. E. Cross and B. J. Nicholson, *Philos. Mag., Ser. 7* **46**, 453 (1955).
- [23] I. Vaskivskiy, I. A. Mihailovic, S. Brazovskii, J. Gospodaric, T. Mertelj, D. Svetin, P. Sutar, and D. Mihailovic, *Nat. Commun.* **7**, 11442 (2016).
- [24] W. Zhong, D. Vanderbilt, and K. M. Rabe, *Phys. Rev. Lett.* **73**, 1861 (1994).
- [25] W. Zhong, D. Vanderbilt, and K. M. Rabe, *Phys. Rev. B* **52**, 6301 (1995).
- [26] I. A. Kornev, L. Bellaiche, P.-E. Janolin, B. Dkhil, and E. Suard, *Phys. Rev. Lett.* **97**, 157601 (2006).
- [27] B. T. Matthias and J. P. Remeika, *Phys. Rev.* **82**, 727 (1951).
- [28] P. Vousden, *Acta Cryst.* **4**, 545 (1951).
- [29] L. Jiang, D. C. Mitchell, W. Dmowski, and T. Egami, *Phys. Rev. B* **88**, 014105 (2013).
- [30] C. I. Cheon, H. W. Joo, K.-W. Chae, J. S. Kim, S. H. Lee, S. Torii, and T. Kamiyama, *Mater. Lett.* **156**, 214 (2015).
- [31] Y. Shiratori, A. Magrez, J. Dornseiffer, F. H. Haegel, C. Pithan, and R. Waser, *J. Phys. Chem. B* **109**, 20122 (2005).
- [32] S. I. Raevskaya, I. P. Raevski, S. P. Kubrin, M. S. Panchelyuga, V. G. Smotrakov, V. V. Eremkin, and S. A. Prosandeev, *J. Phys.: Condens. Matter* **20**, 232202 (2008).
- [33] R. C. Miller, E. A. Wood, J. P. Remeika, and A. Savage, *J. Appl. Phys.* **33**, 1623 (1962).
- [34] J. M. Perez-Mato, D. Orobengoa, M. I. Aroyo, and L. Elcoro, *J. Phys.: Conf. Ser.* **226**, 012011 (2010).
- [35] L. Bellaiche and J. Íñiguez, *Phys. Rev. B* **88**, 014104 (2013).
- [36] S. Prosandeev, D. Wang, W. Ren, J. Íñiguez, and L. Bellaiche, *Adv. Funct. Mater.* **23**, 234 (2013).

- [37] See Supplemental Material at <http://link.aps.org/supplemental/10.1103/PhysRevB.105.L100101> for more details. The goal of this Supplemental Material is fivefold. First of all, we provide information about some model parameters. Second, we schematize the patterns associated with the main local and tilting modes occurring in  $Pca2_1$ ,  $Pc$ , and  $R3c$  phases of NNO. Third, we show the effect of different parameters of the train of electric pulses on the polarization of NNO. Fourth, we demonstrate that the  $Pc$  state is the “natural” state bridging the  $Pca2_1$  and  $R3c$  states, by conducting climbing-image nudged elastic band calculations. Finally, we reveal how strain is also affected by terahertz electric pulses.
- [38] S. Lin, S. Yu, and D. Talbayev, *Phys. Rev. Appl.* **10**, 044007 (2018).
- [39] R. Landauer, *J. Appl. Phys.* **28**, 227 (1957). The reversal of the polarization in ferroelectrics subject to the electric field is thought to require the nucleation of oppositely polarized domains. Experimentally, the nuclei of such domains form thermally, which implies that the activation energy is of several  $k_B T$ . However, according to Landauer’s calculations, the value of this activation is significantly larger because of the large contribution of the depolarizing field to this energy. This contradiction is called Landauer’s paradox.
- [40] B. Xu, V. Garcia, S. Fusil, M. Bibes, and L. Bellaiche, *Phys. Rev. B* **95**, 104104 (2017).
- [41] D. Vanderbilt, *Phys. Rev. B* **41**, 7892 (1990).
- [42] I. Ponomareva, L. Bellaiche, T. Ostapchuk, J. Hlinka, and J. Petzelt, *Phys. Rev. B* **77**, 012102 (2008).
- [43] D. Wang, A. A. Bokov, Z.-G. Ye, J. Hlinka, and L. Bellaiche, *Nat. Commun.* **7**, 11014 (2016).
- [44] T. Tadano and S. Tsuneyuki, *Phys. Rev. B* **92**, 054301 (2015).
- [45] J. P. Perdew, A. Ruzsinszky, G. I. Csonka, O. A. Vydrov, G. E. Scuseria, L. A. Constantin, X. Zhou, and K. Burke, *Phys. Rev. Lett.* **100**, 136406 (2008).
- [46] P. E. Blochl, *Phys. Rev. B* **50**, 17953 (1994).
- [47] G. Henkelman and H. Jónsson, *J. Chem. Phys.* **113**, 9901 (2000).
- [48] G. Henkelman and H. Jónsson, *J. Chem. Phys.* **113**, 9978 (2000).
- [49] G. Mills, H. Jónsson, and G. K. Schenter, *Surf. Sci.* **324**, 305 (1995).
- [50] H. Jónsson, G. Mills, and K. W. Jacobsen, in *Classical and Quantum Dynamics in Condensed Phase Simulations*, edited by B. J. Berne, G. Ciccotti, and D. F. Coker (World Scientific, Singapore, 1998).
- [51] G. Kresse and J. Hafner, *Phys. Rev. B* **47**, 558 (1993).
- [52] G. Kresse and J. Furthmüller, *Phys. Rev. B* **54**, 11169 (1996).
- [53] G. Kresse and D. Joubert, *Phys. Rev. B* **59**, 1758 (1999).
- [54] A. R. Oganov and C. W. Glass, *J. Chem. Phys.* **124**, 244704 (2006).
- [55] A. O. Lyakhov, A. R. Oganov, H. T. Stokes, and Q. Zhu, *Comput. Phys. Commun.* **184**, 1172 (2013).
- [56] A. R. Oganov, A. O. Lyakhov, and M. Valle, *Acc. Chem. Res.* **44**, 227 (2011).
- [57] Z. Wang, S. Joshi, S. Savel’ev, W. Song, R. Midya, Y. Li, M. Rao, P. Yan, S. Asapu, Y. Zhuo, H. Jiang, P. Lin, C. Li, J. H. Yoon, N. K. Upadhyay, J. Zhang, M. Hu, J. P. Strachan, M. Barnell, Q. Wu *et al.*, *Nat. Electron.* **1**, 137 (2018).
- [58] W. Maass, *Neural Networks* **10**, 1659 (1997).
- [59] S. Dutta, V. Kumar, and A. Shukla, *Sci. Rep.* **7**, 8257 (2017).
- [60] V. Milo, G. Malavena, C. M. Compagnoni, and D. Ielmini, *J. Mater.* **13**, 166 (2020).
- [61] S. Boyn, J. Grollier, G. Lecerc, B. Xu, N. Locatelli, S. Fusil, S. Girod, C. Carrétéro, K. Garcia, S. X. J. Tomas, L. Bellaiche, M. Bibes, A. Barthélémy, S. Saighi, and V. Garcia, *Nat. Commun.* **8**, 14736 (2017).
- [62] M. Romera, P. Talatchian, S. Tsunegi, F. A. Araujo, V. Cros, P. Bortolotti, J. Trastoy, K. Yakushiji, A. Fukushima, H. Kubota, S. Yuasa, M. Ernoult, D. Vodenicarevic, T. Hirtzlin, N. Locatelli, D. Querlioz, and J. Grollier, *Nature (London)* **563**, 230 (2018).
- [63] J. Torrejon, M. Riou, F. A. Araujo, S. Tsunegi, G. Khalsa, D. Querlioz, P. Bortolotti, V. Cros, K. Yakushiji, A. Fukushima, H. Kubota, S. Yuasa, M. D. Stiles, and J. Grollier, *Nature (London)* **547**, 428 (2017).
- [64] J. Grollier, D. Querlioz, K. Y. Camsari, K. Everschor-Sitte, S. Fukami, and M. D. Stiles, *Nat. Electron.* **3**, 360 (2020).
- [65] D. Markovic, A. Mizrahi, D. Querlioz, and J. Grollier, *Nat. Rev. Phys.* **2**, 499 (2020).
- [66] R. Khymyn, I. Lisenkov, J. Voorheis, O. Sulymenko, O. Prokopenko, V. Tiberkevich, J. Akerman, and A. Slavin, *Sci. Rep.* **8**, 15727 (2018).
- [67] A. Chakravarty, J. H. Mentinka, C. S. Davies, K. T. Yamada, A. V. Kimel, and Th. Rasinga, *Appl. Phys. Lett.* **114**, 192407 (2019).
- [68] J. Feldmann, N. Youngblood, M. Karpov, H. Gehring, X. Li, M. Stappers, M. Le Gallo, X. Fu, A. Lukashchuk, A. S. Raja, J. Liu, C. D. Wright, A. Sebastian, T. J. Kippenberg, W. H. P. Pernice, and H. Bhaskaran, *Nature (London)* **589**, 52 (2021).
- [69] M. L. Schneider, C. A. Donnelly, I. W. Haygood, A. Wynn, S. E. Russek, M. A. Castellanos-Beltran, P. D. Dresselhaus, P. F. Hopkins, M. R. Pufall, and W. H. Rippard, *Sci. Rep.* **10**, 934 (2020).